THE ASTROPHYSICAL JOURNAL, 317:992–1001, 1987 June 15

SURFACE BRIGHTNESS PROFILES OF 10 COMETS

D. C. JEWITT[1] AND KAREN J. MEECH[1]
Department of Earth, Atmospheric, and Planetary Sciences, Massachusetts Institute of Technology
Received 1986 October 2; accepted 1986 November 25

ABSTRACT

We have used charge-coupled device cameras to measure the radial surface brightness profiles of 10 cometary comae at continuum wavelengths. The surface photometry is accurate to about 1% of the brightness of the night sky. The profiles are conveniently described using the logarithmic derivative $m \equiv d \ln B/d \ln p$, where B is the surface brightness measured at projected distance p from the nucleus. An idealized spherically symmetric, steady-state coma in which the equation of continuity is satisfied would have $m = -1$. The observed comets do not in general conform to this idealized model. Instead, most of the measured comae have steeper surface brightness profiles ($m < -1$) and m decreases monotonically with increasing p. We interpret the steeper profiles using Monte Carlo models in which the distortion of the grain coma by solar radiation pressure is taken into account. The profiles and models suggest that the optically dominant grains are imperfectly dynamically coupled to the sublimated gas. The profiles give no clear evidence for the presence of volatile grains.

Subject headings: comets — photometry

I. INTRODUCTION

Many comets are distinguished by extensive comae comprising solid grains ejected from the nucleus by gas drag. The very low continuum surface brightnesses in such comae indicate that the optical depth due to grains is much less than unity. The radial surface brightness profile in an optically thin coma is given by

$$B(p) = K_1 \int N dl \,, \tag{1}$$

where K_1 is a constant which depends on the size and scattering efficiency of the grains, N (m^{-3}) is the number density of the grains at each point along the line of sight, and dl is an element of length along the line of sight. Here, $p = (x^2 - l^2)^{1/2}/\Delta$ is the projected angular distance from the nucleus measured in the plane of the sky, where x is the radial distance from the nucleus to any point on the line of sight, and Δ is the geocentric distance. Models of the surface brightness distribution may be calculated from equation (1) provided the spatial variation of the number density, N, is specified (e.g., Eddington 1910; Wallace and Miller 1958). Conversely, measurements of $B(p)$ may be used to constrain the spatial dependence of N through the inversion of equation (1).

A particularly simple form for $B(p)$ applies to the special case of a symmetric coma produced by a source of constant strength. Provided the grains move with respect to the nucleus at a constant velocity v and do not change their scattering properties (for instance, as a result of gradual sublimation of ice from their surfaces), the equation of continuity, $N(x)vx^2 =$ constant, guarantees that the number density must decline with distance from the nucleus as $N(x) \propto x^{-2}$ (i.e., the inverse square law prevails). Substitution into and integration of equation (1) then gives $B(p) = K_2/p$, where K_2 is a constant; the local surface brightness varies with the reciprocal of the projected distance in the plane of the sky. We employ the logarithmic derivative

$$m = d \ln B(p)/d \ln p \tag{2}$$

as a convenient measure of the radial surface brightness profile. For the simple steady-state coma described here, $m = -1$.

This well-known result is widely *assumed* to apply to the grain comae of comets. However, there are very few observations against which the assumption may be tested. Several processes, including solar radiation pressure, the sublimation of ice grains, and variable mass loss from the nucleus may all give rise to coma profiles with gradients different from $m = -1$. The need to obtain accurate coma photometry at surface brightnesses equal to a small fraction of the brightness of the night sky constitutes a formidable observational challenge and is no doubt partly responsible for the dearth of published profile measurements. Linear two-dimensional photometers, of a kind available only in the last decade, are virtually a prerequisite for this work. Crude photometry through diaphragms of different diameters has shown that the $m = -1$ law is obeyed locally in some comets (see, e.g., Becklin and Westphal 1966) but not in all (e.g., Newburn, Bell, and McCord 1981; Jewitt and Meech 1985). Profiles of three comets determined using a charge-coupled device (CCD) were presented by Jewitt *et al.* (1982). Only one of the comets showed the canonical $m = -1$ gradient; the other two profiles steepened ($m < -1$) toward large radii. Profiles of additional comets were reported in abstracts by Baum, Millis, and Kreidl (1983) and Baum and Kreidl (1984, 1986); no other high-resolution measurements of the continuum profiles of comets are known to the authors.

Our interest in the profiles is threefold. First, the radial surface brightness profile of a comet is a basic property and provides a direct measure of the grain column density along the line of sight. By way of models, the profile can be used to deduce information about the spatial variation of the number density of the grains. Second, the radial surface brightness variation has practical value if, as is often desired, photoelectric data taken on a single comet with different diaphragms are to

[1] Visiting Astronomer, Kitt Peak National Observatory, National Optical Astronomy Observatories, operated by the Association of Universities for Research in Astronomy, Inc., under contract with the National Science Foundation.

be correctly scaled and compared. Third, in a separate project we are investigating the grain coma of P/Halley, and we wish to know whether the surface brightness characteristics of that comet are in any sense typical of comets as a group.

In this paper we examine the continuum surface brightness profiles of 10 comets measured with CCD detectors. We confine our attention to the radial profiles and so implicitly ignore any azimuthal coma structure which may be present. In a future paper (Meech and Jewitt 1987), we will present coma models which attempt to reproduce the full two-dimensional isophotes of these continuum comets.

II. OBSERVATIONS

The present observations were taken using the 4 m and 2.1 m telescopes at Kitt Peak National Observatory. In 1985 September, the 4 m was used with an 800 × 800 pixel Texas Instruments CCD (TI No. 2) at the f/2.6 prime focus. The image scale was 0".29 per 15 μm pixel, giving a field of view 230" on a side. In 1986 March, the 2.1 m was used with a similar CCD of the same specifications and manufacture (TI No. 3) placed at the f/7.7 Cassegrain focus. The output from the CCD at the 2.1 m was stored in 2 × 2 pixel averaging mode (that is, the chip had 400 × 400 effective pixels), in order to reduce the degree of oversampling of the instrumental point-source function. The resulting image scale was 0".38 per 30 μm effective pixel, and the field of view was 150" on a side. Both chips had a root mean square readout noise of about 18 electrons. Sensitivity variations among the pixels on each CCD were removed using flat-field exposures taken each night on the illuminated interior of the observatory dome. The overclock bias level of the CCD was measured at the end of each exposure. The reduced images were photometrically calibrated using standard stars from the lists by Oke and Gunn (1983) and Christian *et al.* (1985).

Images of comets P/Giacobini-Zinner, P/Giclas, P/Shoemaker 3, P/Maury, P/Kojima, P/Halley, P/Daniel, P/Whipple, P/Gehrels 3, and P/Gunn were obtained (Fig. 1; Pl. 15). These comets were all small in comparison with the field of view, so that the instantaneous brightness of the night sky could be determined from the individual CCD images. Pertinent parameters of the images used to compute the profiles discussed in this work are given in Table 1. The seeing on each night was 1"–1".5 full width at half-maximum (FWHM) at the 4 m and 2"–2".5 FWHM at the 2.1 m. The telescopes were autoguided on field stars and differentially tracked at cometary rates during each integration. However, experiments proved that neither of the Kitt Peak telescopes were able to consistently reproduce the motions of the comets to better than ~1". Consequently, the innermost regions of each profile ($p < 3$") are affected by image smear as well as by seeing. The two comets known (from spectroscopy) to possess significant gaseous emission (P/Giacobini-Zinner and P/Halley) were imaged using a narrow-band continuum filter centered at $\lambda = 7005$ Å and $\Delta\lambda = 89$ Å FWHM. The remaining comets were imaged through the Mould R ($\lambda = 6500$ Å, FWHM = 1280 Å) filter. Comets P/Maury, P/Giclas, P/Daniel, P/Gehrels 3, and P/Gunn were also imaged in the Mould V ($\lambda = 5460$ Å) filter. The V and R filter profiles were found to be identical within the uncertainties of measurement (consistent with the continuum nature of these comets). Therefore, we restrict the following discussion to profiles measured in the R and continuum filters.

The radial surface-brightness profiles were computed by averaging the coma signal within concentric annuli about each photometric center. The averaging algorithm took proper photometric account of those pixels which straddled the boundaries between annuli. The contents of bad pixels were replaced by the average of the signals in adjacent pixels. Uncertainties in the coma profiles were dominated by the uncertainty in the brightness of the night sky. Statistical uncertainties in the local sky level were typically of order 0.1%, on scales of a few tens of pixels on the CCD. However, on scales of a few hundred pixels (comparable to the projected dimensions of the larger comets), the sky level was observed to undulate with a considerably larger range. These larger undulations most probably result from small differences between the flat field and the sky illumination. The large-scale uncertainties were estimated in two ways. First, examination of images of stellar fields showed that the detector response was independent of position on the CCD to better than 1% peak-to-peak over the full width of the chip. Second, measurements of the sky brightness at different positions around each comet were consistent to better than 0.6% peak-to-peak in every case. For our present purposes we estimate the 1 σ sky brightness uncertainty as $\pm$1% of the mean. This is probably an overestimate of the sky uncertainty around the smaller comets. Empirical evidence for the linearity of the CCD response was provided by the invariance of the coma profiles with respect to the signal level in images taken with different exposures, as well as by the internal consistency of the standard star photometry.

The surface brightness profiles are shown in Figure 2*a–j*. The profiles are plotted on a common scale to facilitate direct

TABLE 1

JOURNAL OF OBSERVATIONS

Comet	Date	UT[a]	Telescope	Filter	Airmass	Exposure (seconds)
P/Giacobini-Zinner	1985 Sep 23	12:20	4 m	7005 Å	1.18	30
P/Giclas	1985 Sep 21	10:17	4 m	*R*	1.13	15
P/Shoemaker 3	1986 Mar 5	05:32	2.1 m	*R*	1.02	600
P/Maury	1985 Sep 22	05:10	4 m	*R*	1.29	150
P/Kojima	1986 Mar 5	06:13	2.1 m	*R*	1.11	450
P/Halley	1985 Sep 21	10:04	4 m	7005 Å	1.54	100
P/Daniel	1986 Mar 6	08:25	2.1 m	*R*	1.01	300
P/Whipple	1985 Sep 22	07:14	4 m	*R*	1.69	150
P/Gehrels 3	1986 Mar 6	10:31	2.1 m	*R*	1.71	300
P/Gunn	1985 Sep 22	10:09	4 m	*R*	1.21	120

[a] Universal Time of the middle of the integration.

comparisons among the comets. The surface brightness units are *R* filter magnitudes per square arcsecond, except for comets P/Halley and P/Giacobini-Zinner, for which the magnitudes are in the AB_{79} system of Oke and Gunn (1983). Practically, $AB_{79} \approx V$ for an object with a flat spectrum. The brightness of the night sky near each comet is indicated in Figure 2 by a horizontal bar on the right-hand axis. The error bars in the figure illustrate the effect on the profiles of changing the adopted sky brightness by $\pm 1\%$. The plotted errors are thus systematic in nature; the statistical errors in each profile may be estimated from the local scatter of the individual measurements. Generally, the sky subtraction uncertainty has an important effect on a profile only at the largest measured radii. Occasional bumps and gaps in the plotted profiles are due to incomplete field star subtraction. Diagonal lines in the lower left of each panel of Figure 2 indicate gradients $m = -1$ and $m = -3/2$ for visual reference.

The variation of the logarithmic gradient with radius is shown in Figure 3*a–b*. The gradient was computed by differentiating polynomials fitted to the profiles in Figure 2. Vertical bars in the figure show the uncertainty in the value of *m* at each radius caused by the $\pm 1\%$ sky subraction uncertainty discussed above. Points at projected radii $\log p < 0.5$ and points at which the gradient uncertainty is $\Delta m > \pm 0.5$ have not been plotted.

III. INTERPRETATION AND DISCUSSION

a) Qualitative Remarks

The comet profiles shown in Figure 2 share a number of qualitative similarities. Most noticeably, the profiles are smooth and monotonically decreasing functions of increasing radius, with little evidence for small-scale structure. The regions in the profiles where $p \leq 3''$ ($\log p \leq 0.5$) are rounded due to the combined effects of the atmospheric seeing (1″–2″.5), the imperfect telescope tracking (<1″), and the spatial quantization imposed on the images by the CCD pixel grid (0″.3–0″.4). Beyond the seeing disks ($0.5 < \log p < 1.0$), several comae exhibit local gradients $m \approx -1$ (see comets P/Giacobini-Zinner, P/Maury, P/Shoemaker 3, and P/Daniel in Fig. 2), but *m* typically decreases at larger radii. The gradients of most profiles (P/Whipple, P/Halley, and P/Giacobini-Zinner are exceptions) lie in the range $-3/2 \leq m \leq -1$, and most exhibit negative curvature ($dm/d \ln p < 0$). Thus, Figure 3 shows that the frequently assumed $m = -1$ gradient provides only a crude approximation to the comae of the observed comets.

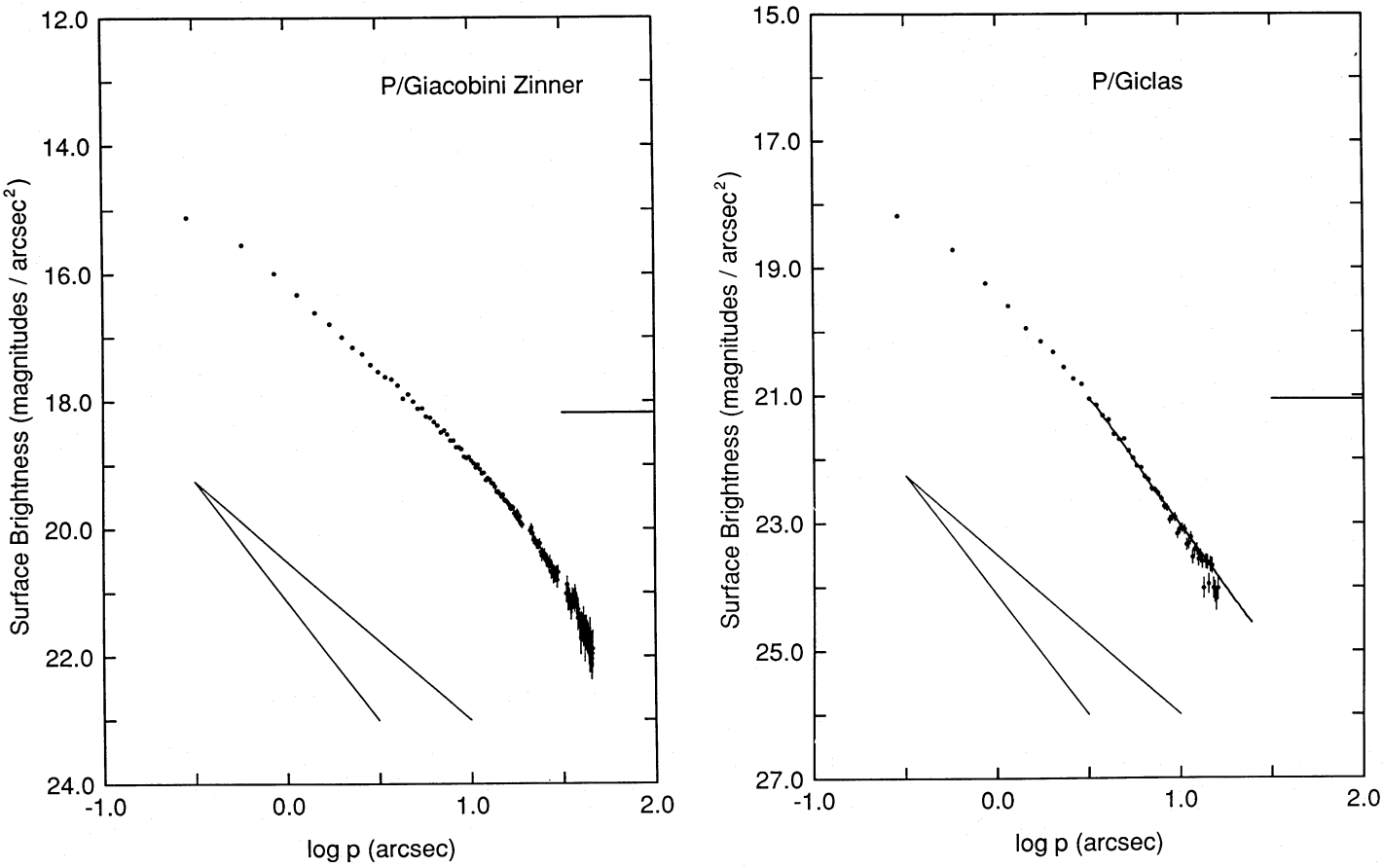

FIG. 2.—The continuum surface brightness profiles of 10 comets. The surface brightness (in *R* filter magnitudes per square arcsecond unless otherwise noted in the text) is plotted against the logarithm of the radius (in arcseconds) of the center of the annulus within which the surface brightness was determined. The brightness of the night sky is marked in each panel by a short horizontal bar on the right-hand axis. Diagonal lines in the lower left of each plot indicate gradients $m = -1$ and $m = -3/2$. Continuous lines drawn through the data represent radiation pressure models computed according to the procedures described in § III*b*. The models apply to $\log p \geq 0.5$. Error bars illustrate the *systematic* (as opposed to statistical) uncertainty in each profile which would be caused by a $\pm 1\%$ error in the determination of the surface brightness of the night sky. The geometrical parameters of the comets at the time of observation may be read from Table 2. The parameters of the models (where shown) may be read from Table 3.

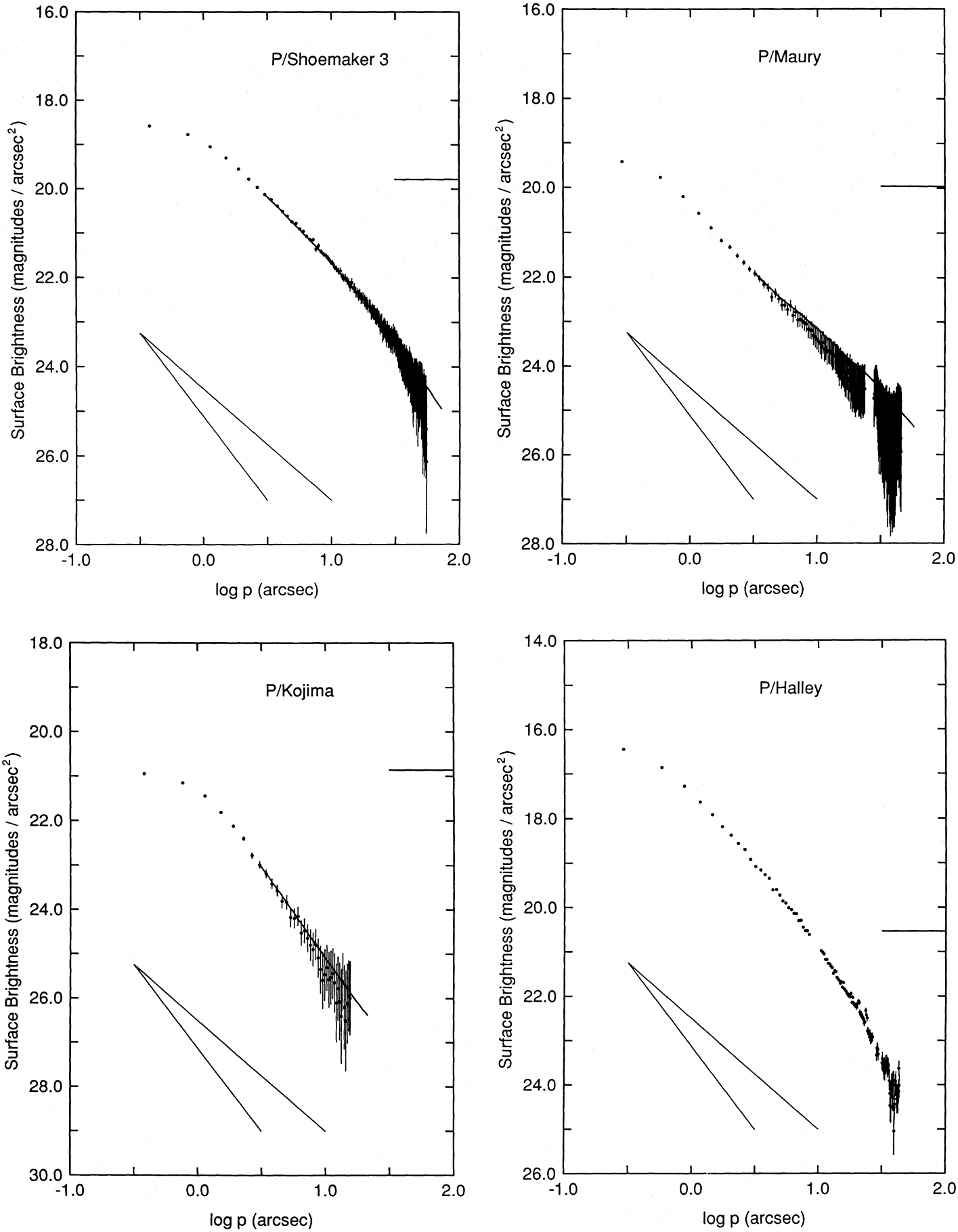

FIG. 2.—*Continued*

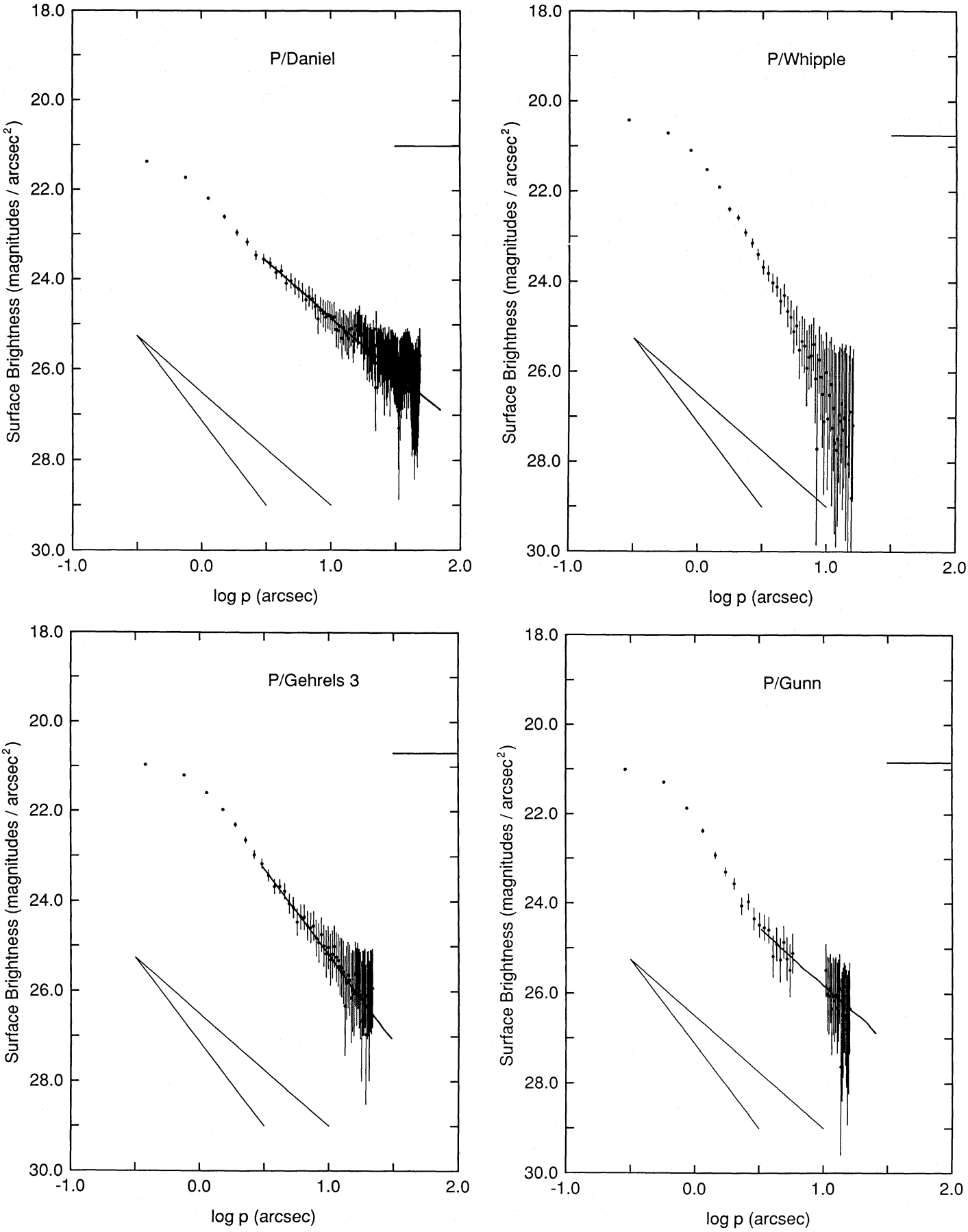

FIG. 2.—*Continued*

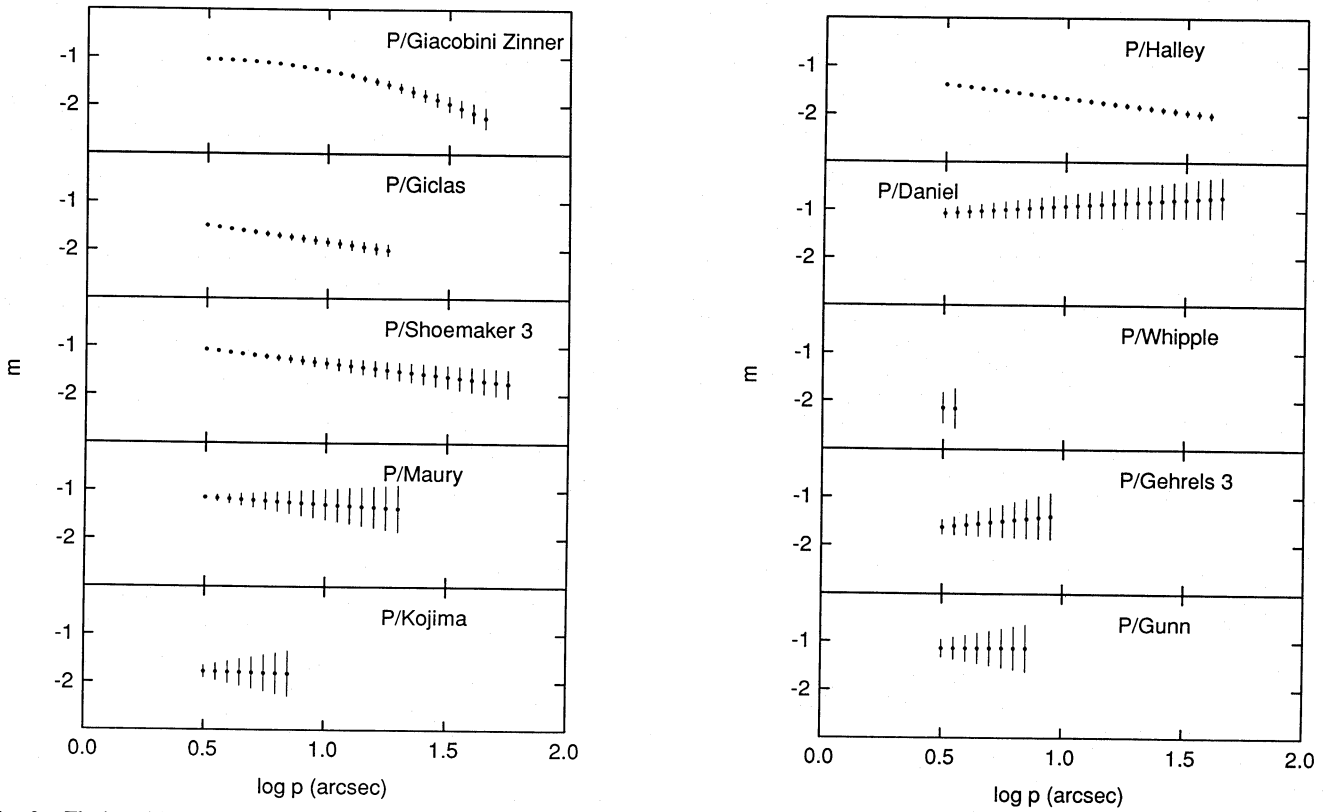

FIG. 3.—The logarithmic gradient m is plotted against the logarithm of the projected radius (in arcseconds). Vertical bars represent the systematic uncertainties in m due to the $\pm 1\%$ background subtraction uncertainty. The plots are terminated at low surface brightness (large p) where the uncertainty in the gradient exceeds ± 0.5, or where the photometry ends, whichever comes first. A steady-state coma in uniform expansion would plot as a horizontal line at $m = -1$. Only the comae of P/Maury, P/Gunn, and P/Daniel are consistent with this simple behavior, within the uncertainties of measurement.

Two length scales of physical interest must be mentioned in connection with the interpretation of the profiles in Figure 2. First, the grains are accelerated to terminal velocity in a finite zone around the nucleus. In this "acceleration zone," we expect that the grain number density should deviate from the inverse square law, giving rise to a steep brightness gradient near the nucleus. The linear dimension of the acceleration zone, X_A, can be estimated from the condition that, in order to be accelerated to a significant fraction of the gas speed, a grain must be hit by a mass of gas molecules at least comparable to its own mass. When applied to a grain of radius $a(m)$ and density ρ (kg m^{-3}), this condition gives

$$X_A \approx \rho a/(\mu m_H N) , \quad (3)$$

where $\mu = 18$ is the molecular weight of the sublimated molecules (mostly H_2O), $m_H = 1.67 \times 10^{-27}$ kg is the mass of the hydrogen atom, and N is the gas number density at the nucleus. The approximate surface-number density may be calculated from $N \approx Q/(4\pi v r_n^2)$, in which $Q \approx 10^{29}$ s^{-1} (Weaver *et al.* 1981) is the production rate from an active nucleus of radius $r_n = 10^3$ m at $R = 1$ AU and v is the velocity of expansion of the gas. The empirical Bobrovnikoff/Delsemme law (Delsemme 1982) gives the velocity as v_B (m s^{-1}) $\approx 600R^{-1/2}$ or $v_B \approx 600$ m s^{-1} at $R = 1$ AU (the speed of sound in gaseous water at a temperature appropriate to this R is also $v \approx 600$ m s^{-1}). By substitution, we find $N \approx 10^{19}$ m^{-3}. The size of the acceleration zone for representative grains ($a = 10^{-6}$ m and $\rho = 10^3$ kg m^{-3}) is then $X_A \approx 3 \times 10^3$ m (or $X_A \approx 3r_n$), rising to $X_A \approx 3 \times 10^4$ m ($X_A \approx 30r_n$) for $a = 10^{-5}$ m. Evidently, the acceleration zone is rather small.

On a larger scale, solar radiation pressure limits the extent of the grain coma in the sunward direction to a distance of order

$$X_R \approx v_{gr}^2 R^2/[2\beta g_{sun}(1)] , \quad (4)$$

where β is the ratio of the acceleration of a grain due to radiation pressure to the local solar gravity, $g_{sun}(1) = 0.006$ m s^{-2} is the solar gravity at $R = 1$ AU, and v_{gr} (m s^{-1}) is the terminal ejection velocity of a grain. Current wisdom has it that the empirical Bobrovnikoff/Delsemme law should provide a reasonable approximation to the grain terminal speed (i.e., $v_{gr} \approx v_B$), as the optically dominant micron-sized grains should be well coupled to the gas, at least near $R \approx 1$ AU. Equation (4) then gives $X_R \approx 3 \times 10^7 R/\beta$. The coma of a comet at $R = 1$ AU, containing grains with $\beta \approx 1$, would have the order of magnitude length scale $X_R \approx 3 \times 10^7$ m. Viewed from geocentric distance $\Delta = 1$ AU, this length subtends 40″, and so is quite comparable to the observed dimensions of the comets in this study (see Fig. 1).

The scales X_A and X_R conveniently divide the grain coma into four distinct regions.

Region 1.—On length scales $x < X_A$ the surface brightness is sensitive to the details of the grain acceleration process. At $\Delta = 1$ AU, the angle subtended by X_A is $X_A/\Delta \approx 0\farcs04$, far smaller than the typical 1″ ground-based resolution. However, although the acceleration zone is unresolvable from the ground, the grains in it may nevertheless contribute to the

coma profile within the central seeing disk. Likewise, the solid nucleus is unresolved (angular diameter of order 10^{-3}″) but may also contribute to the central surface brightness profile. A good example is provided by the surface brightness profile of comet P/Arend-Rigaux (Jewitt and Meech 1985), which showed a strong central spike, due to the unresolved nucleus, rising above a faint extended coma. In principle, information about the distribution of dust in region 1 could be extracted from numerical deconvolutions of the central surface-brightness profiles shown in Figure 2, using the profiles of nearby stars. Unfortunately, the comet rate tracking errors (§ II) render the results of deconvolution uncertain. In this paper, we ignore the parts of the profiles with $p < 3''$.

Region 2.—On the length scales in the range $X_A \ll x \ll X_R$, the effects of gas drag and radiation pressure are both small and the surface brightness gradient should be near $m = -1$. This is especially well seen in the profiles of P/Giacobini-Zinner, P/Shoemaker 3, and P/Maury (Figs. 2 and 3).

Region 3.—On length scales $x \approx X_R$, surface photometry may be expected to yield information about the magnitude of the radiation pressure acceleration, β, which is itself a function of $Q_{pr}/(\rho a)$, where the radiation pressure efficiency, Q_{pr}, depends on the grain size, shape, and composition. For instance, the simplest measure of the radiation pressure is provided by the length of the sunward extension of the coma through equation (4). The present study is concerned mostly with region 3.

Region 4.—On scales $x \gg X_R$ the coma becomes highly distorted by radiation pressure and is traditionally renamed as the "type II tail." The shape and orientation of the tail may be used in syndyne/synchrone analyses to constrain the characteristics of the tail grains and their source. Detailed attempts to match tail isophotes have been published for comets Arend-Roland (Finson and Probstein 1968), Seki-Lines (Jambor 1973), and Bennett (Sekanina and Miller 1973). A disadvantage of the dynamical analysis when applied to region 4 is that the grain flight time for tail particles may be comparable to the time scale for change of the heliocentric distance, so that time dependence of the grain source function must be added to the already considerable number of free parameters in the model.

b) *Radiation Pressure Model*

A Monte Carlo computer program was written to calculate surface brightness profiles of cometary comae by accounting for solar radiation pressure and for various adopted nucleus source functions. The aim of the calculation was to mimic the observed surface brightness profiles using simple physical models of the coma. The simplicity and versatility of the Monte Carlo method led us to use it in preference to the direct integration of equation (1) (see Wallace and Miller [1958] for examples of the latter method).

In the model, a preselected number of grains, η, are ejected with velocity v_{gr}, and the location of each grain with respect to the nucleus is calculated and recorded at a selected number of subsequent times. The model assumes steady state and does not treat the initial grain acceleration by gas drag and so does not apply to region 1. The model neglects the effects of the relative orbital motions of the grains about the Sun, as these effects are small compared to the effects of radiation pressure within the inner coma considered here. The probability that a grain will be ejected in direction φ, ϕ is given by the source function, $S(\varphi, \phi)$, which is normalized so that $\iint \sin \varphi S(\varphi, \phi) d\varphi d\phi / 4\pi = 1$. Most calculations were done with isotropic [$S(\varphi, \phi) = 1$] or half isotropic [$S(\varphi, \phi) = 1$ for $|\varphi| \leq \pi/2$, $|\phi| \leq 2\pi$; $S(\varphi, \phi) = 0$ otherwise] source functions corresponding to isothermal and half isothermal spherical nuclei. Although we have no reason to expect that real nuclei are either spherical or isothermal, test calculations done using more complicated source functions show that the brightness profiles are not very sensitive to the exact form of the adopted source function, except close to the nucleus.

The effective surface brightness of the model coma was taken to be proportional to the number of grains projected per unit area in the plane of the sky. The model grains were counted in concentric annuli corresponding to the photometry annuli used on the real data. Each calculation was continued for a time large enough to ensure that even the slowest grain had escaped from the largest counting annulus. The calculations were performed with numbers of grains and sample times sufficient to give good signal-to-noise ratio at all radii; for example, 10^4–10^5 grain positions were usually sufficient for models with 5″ resolution.

The profiles computed from the radiation pressure model depend on the length X_R and on the phase angle θ. For a given heliocentric distance, X_R is proportional to v_{gr}^2/β (eq. [4]). Thus the model cannot be used to find either v_{gr} or β separately, but only the value of v_{gr}^2/β which gives the best fit to the data. Both v_{gr} and β are poorly known functions of the particle size. In real comets, the grains are likely to populate a wide distribution of sizes, leading to a range of values of v_{gr}^2/β within each coma. We simulate the effects of the grain size distributions by summing the models over broad distributions in X_R, with fractional widths $\Delta X_R/X_R \leq 2$. Our tests show that the shapes of the model profiles are insensitive to the details of the smoothing.

Profiles of model comae are shown in Figure 4. The figure shows the effect on the profile of varying X_R, while keeping the phase angle constant at $\theta = 90°$. The heliocentric and geocentric distances are set equal to unity and an isotropic source function is used. For clarity, the profiles are plotted with arbitrary vertical offsets. Small bumps on the curves are due to noise in the computer model and can be reduced to an arbitrarily small level (though at increasingly large computing expense) by increasing the number of particles in the calculation. As the radiation pressure approaches zero (i.e., $X_R \to \infty$) the logarithmic gradient approaches $m = -1$; as expected, the spherical, steady-state coma is just a limiting case of the radiation pressure model. With growing radiation pressure, the profile develops significant curvature and steepens at its outer edge ($dm/d \ln p < 0$). A broad bend develops in the profile at the projected radius $p = X_R/\Delta$. The outer part of the profile has the gradient $m = -3/2$, while the inner part retains $m = -1$. The location of the bend between the $m = -1$ and $m = -3/2$ portions moves outward with increasing X_R, following equation (4).

Figure 5 shows the effect of the viewing geometry on the surface brightness profile of a model comet. The profiles refer to a comet at $R = \Delta = 1$ AU viewed at phase angles in the range $0 \leq \theta \leq 90°$, with $X_R = 1.5 \times 10^7$ m (20″). The profiles are symmetric about $\theta = 90°$. The profile for $\theta = 0$ has the $m = -1$ gradient of a symmetric steady-state coma, as radiation pressure then acts parallel to the line of sight, and the motions of the grains in the plane of the sky are unaccelerated. The models at $\theta > 0$ show the negative curvature ($dm/d \ln p < 0$) which is a characteristic of the profiles of many real

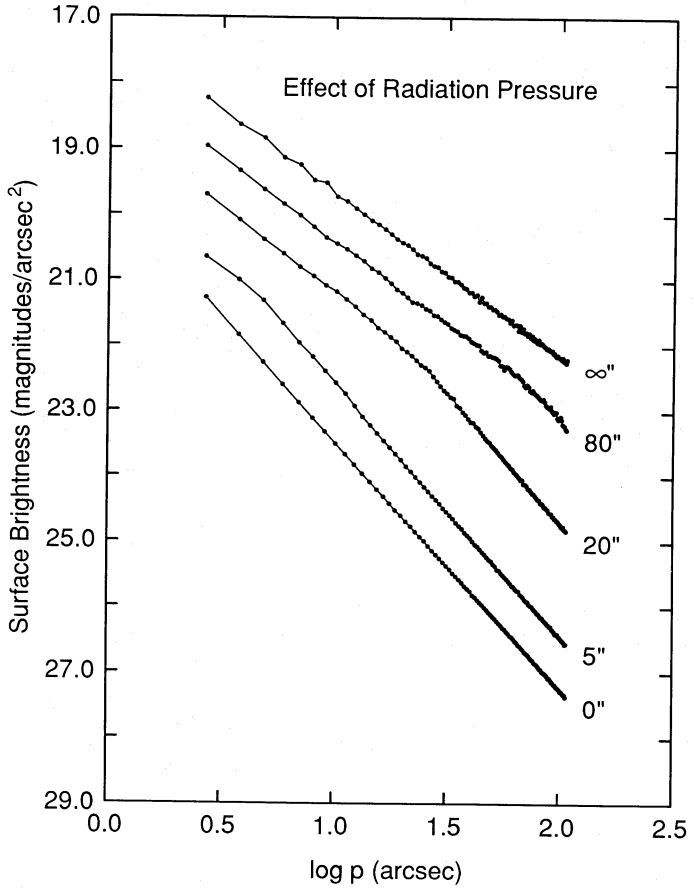

FIG. 4.—Sample surface brightness profiles of Monte Carlo model comae are shown as a function of the dimension X_R (expressed in arcseconds). The parameter provides a measure of the importance of radiation pressure to the shape of the coma. Successive profiles have been vertically offset for clarity and the zero point of the vertical axis was arbitrarily chosen. The models have 1″ resolution and refer to a comet at $R = \Delta = 1$ AU viewed from phase angle $\theta = 90°$. Each model has been integrated over a small range of values of X_R in the real comets. Calculated points are shown by dots, while connecting lines have been added for clarity. Note that the gradient $m \to -1$ as $X_R \to \infty$ and $m \to -1.5$ as $X_R \to 0$.

comets (cf. Figs. 2 and 5). As the coma is viewed from successively larger phase angles, the outer portion ($\log p > 1.5$) becomes increasingly steep, ultimately reaching $m = -3/2$ at $\theta = 90°$. The location of the knee which connects the $m = -1$ and $m = -3/2$ portions of the $\theta = 90°$ profile in Figure 5 again corresponds to the angle subtended by X_R (eq. [4]). The portion of the profile inside the knee retains a slope $m = -1$ independent of the phase angle. This result, that the $m = -1$ gradient is invariant with respect to phase angle inside the critical distance X_R, was first demonstrated in numerical calculations by Wallace and Miller (1958).

The origin of the $m = -3/2$ limit to the model gradient may be understood as follows. Provided the width of the tail is small compared to the radius of the annulus within which the surface brightness is determined, the number of grains within the annulus can be written $J = \Delta T dJ/dt$. Here, dJ/dt is the number of grains passing through any plane perpendicular to the tail axis per second and $\Delta T = \Delta p/u$ is the time taken for a grain to cross the annulus of projected radial width Δp. In steady state we may take dJ/dt = constant, since grains may neither accumulate in nor deplete from any segment of the tail. The grain velocity along the tail due to radiation pressure is approximately $u \propto (2\beta g_{\rm sun} p)^{1/2}$ (for $u \gg v_{\rm gr}$), so that $J \propto p^{-1/2}\Delta p$. The surface brightness $B(p)$ is proportional to the number of grains J in the annulus divided by the area of the annulus, $2\pi p\Delta p$. Therefore, the annular surface brightness in the tail should vary as $B(p) \propto p^{-1/2}\Delta p/(2\pi p\Delta p)$ or $B(p) \propto p^{-3/2}$, as is seen in the numerical models. The preceding argument, given here for the case of a single radiation pressure factor β is also valid when applied to more realistic models in which a β distribution is included.

The apparent similarity between the measured profiles on the one hand (Fig. 2), and the model profiles on the other (Figs. 4–5), encourages us to attempt to fit the models to the measurements. Representative results of these attempts are shown by continuous lines through the data in Figure 2. Models were calculated for each comet using values of R, Δ, and θ from Table 2. The magnitude of X_R was varied to achieve the best fit to each profile. No attempt was made to fit the points having $\log p < 0.5$, these being affected by seeing and image trailing in each profile. Profiles of comets P/Giclas, P/Shoemaker 3, P/Maury, P/Kojima, P/Daniel, P/Gehrels 3, and P/Gunn can all

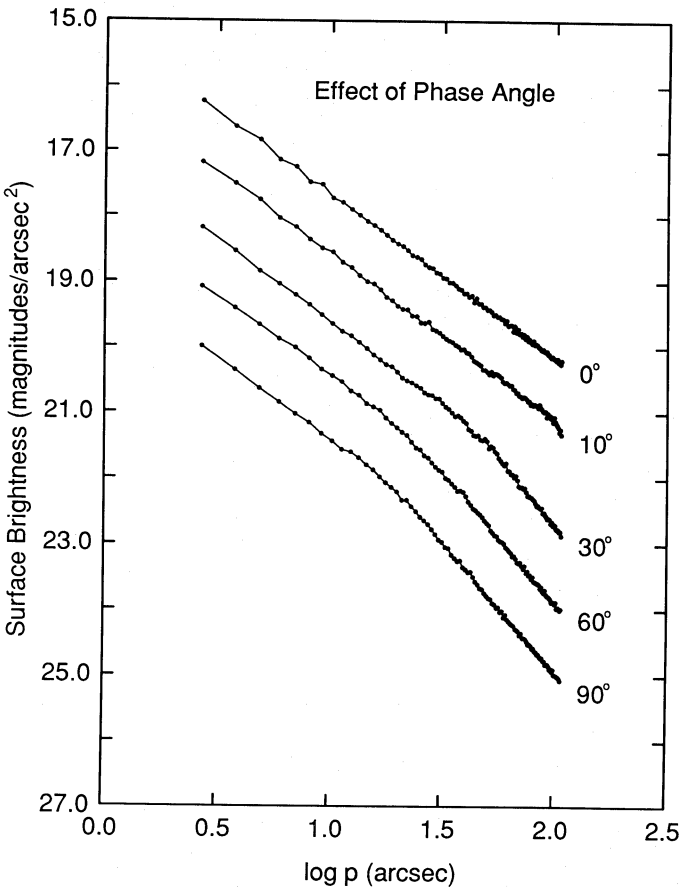

FIG. 5.—The surface brightness profile of a particular Monte Carlo model coma as a function of the phase angle θ. Successive profiles have been vertically offset for clarity and the zero point of the vertical axis was arbitrarily chosen. Each profile was derived from about 10^5 calculated grain positions. The calculations refer to a comet at $R = \Delta = 1$ AU, with $X_R = 1.5 \times 10^7$ m (corresponding to 20″). Profiles computed for other values of X_R show qualitatively similar dependence on the phase angle. Each model has been integrated over a small range of values of X_R in order to simulate the smoothing effects of a grain size distribution in the real comets.

TABLE 2

GEOMETRY OF THE COMETS

Comet	R (AU)	Δ (AU)	θ	Scale (m/″)
P/Giacobini-Zinner	1.06	0.51	69°.6	3.71×10^5
P/Giclas	1.84	1.04	25.5	7.56×10^5
P/Shoemaker 3	1.98	1.05	14.0	7.64×10^5
P/Maury	2.21	1.31	14.6	9.53×10^5
P/Kojima	2.42	1.65	17.9	1.20×10^6
P/Halley	2.47	2.35	23.9	1.71×10^6
P/Daniel	2.55	1.66	12.0	1.21×10^6
P/Whipple	3.36	2.52	10.9	1.83×10^6
P/Gehrels 3	3.58	2.59	2.6	1.88×10^6
P/Gunn	4.64	4.37	12.4	3.18×10^6

be fitted, within the uncertainties of measurement, by plausible radiation pressure models (Fig. 2). Within the uncertainties of measurement, only three of the comets (P/Maury, P/Gunn, and P/Daniel) have profiles consistent with the canonical $m = -1$ model.

Table 3 lists representative values of X_R and $v_{gr}{}^2/\beta$ for each comet to which a fit was possible (comet P/Gunn is omitted from the table as its uncertain profile does not strongly constrain X_R). We also list v_B, the Bobrovnikoff velocity for the heliocentric distance of each comet, and $v_1 = (v_{gr}{}^2/\beta)^{1/2}$. Studies of the tails of comets (e.g., Saito *et al.* 1981) show that most grains have $\beta < 1$, so that v_1 constitutes a practical upper limit to the terminal velocity of the grains. In every case where the radiation pressure model provides an acceptable fit to the data, we find $v_1 < v_B$; the grain terminal velocity inferred from the surface brightness profiles is smaller than the speed computed from the modified Bobrovnikoff relation. The Bobrovnikoff speed is deduced from observations of expanding halos in the inner comae of comets and is probably close to the speed of expansion of the sublimated gas (Delsemme 1982). Therefore, the inequality $v_1 < v_B$ gives evidence that the grains in the comets of this study are imperfectly coupled to the gas, a result consistent with the rapidly declining flux of water molecules at distances $R \geq 2$ AU.

The profiles of comets P/Halley, P/Whipple, and P/Giacobini-Zinner are too steep at large radii to be compatible with the basic radiation pressure model. Models computed using arbitrarily complex source functions fail to improve the agreement with the steep profiles. We must seek other reasons for the apparent failure of the radiation pressure model in these three comets.

c) *Other Models*

Two major assumptions used in the above radiation pressure models are (1) that the coma is produced in steady state and (2) that the grains in the coma do not change their optical characteristics with increasing distance from the nucleus. We briefly consider the consequences of relaxing these assumptions.

TABLE 3

PARAMETERS OF FITTED MODELS

Comet	X_R (m)	$v_{gr}{}^2/\beta$ (m^2 s^{-2})	V_B (m s^{-1})	v_1 (m s^{-1})
P/Giclas	$< 1.6 \times 10^6$	$< 5.6 \times 10^3$	440	< 75
P/Shoemaker 3	$(7.4–15) \times 10^6$	$(2.2–4.5) \times 10^4$	430	150–210
P/Maury	$> 2.3 \times 10^6$	$> 5.6 \times 10^3$	400	> 75
P/Kojima	$< 1.4 \times 10^6$	$< 2.8 \times 10^3$	385	< 50
P/Daniel	$> 3.1 \times 10^6$	$> 5.6 \times 10^3$	375	> 75
P/Gehrels	$< 2.4 \times 10^7$	$< 2.3 \times 10^4$	320	< 150

The surface brightness profile is especially sensitive to variations in the rate of coma production occurring on the grain flight time $\tau \approx v_{gr}/(\beta g_{sun})$. For a canonical comet at $R = 1$ AU, this time is $\tau \approx 10^5$ s (about 1 day). Variations occurring on the time scale τ would produce expanding ripples in the coma with a wavelength $w \approx v_{gr}\tau \approx X_R$, whereas variations on much shorter or longer time scales would produce ripples either too small or too large to be discerned from the profile. Variability in the rate of coma production could be caused by diurnal illumination of active sites on the nucleus and by stochastic surface effects leading to "outbursts." Numerous photometric measurements of P/Halley (by the authors and others) indeed show that its inner coma varied in brightness by a factor ≥ 2 on time scales ≈ 1 day. We suspect that the radiation pressure models fail to match the profile of P/Halley simply because the assumption of steady state is violated. Source variability may also account for the steep profiles of P/Whipple and P/Giacobini-Zinner; however, no time-resolved observations of these comets are available to test this hypothesis. Source variability should produce profiles alternately shallower then steeper than the steady-state profile, depending on the time of observation.

A progressive change in the optical characteristics of the grains with increasing distance from the nucleus could be caused by several processes. The most interesting of these is the possible sublimation of water ice from the grains, which leads to a decrease in grain cross section at larger distances and to a sharp-edged coma. Ice grain sublimation, as it pertains to comets, has been discussed by Delsemme and Miller (1971), by Hanner (1981), and most recently by Mukai (1986).

The main consequence of the presence of sublimating water ice grains is a steep surface brightness profile, *qualitatively* similar to the steep profiles observed in comets P/Giacobini-Zinner, P/Halley, and P/Whipple. However, we are reluctant to embrace the water ice grain halo model as an explanation for the overall profiles of these or other comets for two reasons.

First, the maximum distances reached by dirty water ice grains near $R = 1$ AU are of order 10^4–10^5 m (Hanner 1981; Mukai 1986), whereas the radius of the coma of P/Giacobini-Zinner is greater than 2×10^7 m at $R = 1.06$ AU (see Fig. 2). Therefore, any sublimating water grains in that comet would be confined to a region within the seeing disk and could have no influence on the outer profile. (A few comets [e.g., P/Gunn] show pronounced central bumps which might be due to *near-nucleus* ice grains.) Longer grain lifetimes, and correspondingly larger scale lengths, would result if the grain materials were supposed to be less volatile than water, but the entirely ad hoc nature of this supposition makes it unappealing.

Second, all 10 comets in this study show pronounced antisunward extensions which are clearly due to the action of radiation pressure rather than to ice grain halos. Naturally, it is possible to construct more complicated models which incorporate both solar radiation pressure and sublimating grains, but these models would seem premature in the absence of observational evidence supporting the assumption of steady state. In short, although ice grains may well exist in the comae of comets (Mukai 1986), we do not yet possess sufficient data to distinguish them from the effects of solar radiation pressure and/or possible variations in the coma source strength.

A different conclusion about sublimating grains has been

advanced in a recent abstract by Baum and Kreidl (1986). These authors ignore the effects of radiation pressure; instead they interpret all surface brightness deviations from the $m = -1$ law as evidence for the presence of volatile grains. We merely comment that, while the very existence of volatile grains in comet comae is controversial, the physical importance of radiation pressure is demonstrated beyond reasonable doubt by the existence of the dust tails, and by the characteristic asymmetry of the typical cometary coma. Reasonable claims for the presence of volatile grains can be made only after the effects of solar radiation pressure have been taken into account.

IV. CONCLUSIONS

1. The continuum radial surface brightness profiles of 10 comets have been measured from charge-coupled device images, with surface photometry accurate to about 1% of the brightness of the night sky. Except in a limited central region, a majority of the coma profiles are steeper than the canonical $m = -1$ profile anticipated from a symmetric, steady-state coma source.

2. Seven of the 10 measured comets (P/Giclas, P/Shoemaker 3, P/Maury, P/Kojima, P/Daniel, P/Gehrels 3, and P/Gunn) show profiles which are consistent with simple models which account for the effects of solar radiation pressure (profiles of P/Maury, P/Daniel, and P/Gunn are also consistent with the absence of radiation pressure, within the uncertainties of measurement). The photometric gradients decrease from $m = -1$ for $x < X_R$ to $m = -3/2$ for $x > X_R$, where X_R is the extent of the coma in the direction toward the Sun, as a result of solar radiation pressure. Differences among the seven profiles result from different values of the scale length X_R, and, to a lesser extent, from differences in the phase angles at which the comets were observed.

3. The upstream scale lengths computed from the profiles imply grain terminal speeds which are less than the Bobrovnikoff speed.

4. Profiles of three comets (P/Halley, P/Whipple, and P/Giacobini-Zinner) have $m < -3/2$ and cannot be fitted by the steady-state radiation pressure models considered here. These steep profiles probably reflect variations in the strength of the nucleus source on time scales comparable to the grain flight time. Such variations in P/Halley are *known* from independent photometry. Time-resolved area photometry will be needed to fully understand the profiles of these comets.

5. The present data provide no clear evidence for a significant population of icy grains in these comets. Icy grains may be present (indeed, we expect them), but their effects on the measured surface brightness profiles are not easily separated from the effects of radiation pressure and of possible source variations. Future time-resolved surface brightness measurements might allow a stronger statement about icy grains.

We thank Dean Hudek for cheerful assistance at both telescopes, Vesa Junkkarinen for a careful introduction to TI No. 2, and Jeannette Barnes for help with the computers at Kitt Peak headquarters. Sid d'Groullicque is thanked for helpful comments. The coma models were computed on the Planetary Astronomy VAX at MIT. This work was undertaken in support of our research on comet P/Halley, funded by a grant from the NASA Planetary Astronomy Program.

REFERENCES

Baum, W. A., and Kreidl, T. J. 1984, *Bull. A.A.S.*, **16**, 643.
———. 1986, in *Asteroids, Comets, Meteors II*, ed. C. Lagerkvist, B. Lindblad, H. Lundstedt, and H. Rickman (Uppsala: Uppsala University Press), p. 397.
Baum, W. A., Millis, R. L., and Kreidl, T. J. 1983, *Bull. A.A.S.* **15**, 801.
Becklin, E. E., and Westphal, J. A. 1966, *Ap. J.*, **145**, 445.
Christian, C. A., Adams, M., Barnes, J. V., Butcher, H., Hayes, D. S., Mould, J. R., and Siegel, M., 1985, *Pub. A.S.P.*, **97**, 363.
Delsemme, A. H. 1982, in *Comets*, ed. L. L. Wilkening (Tucson: University of Arizona Press), p. 85.
Delsemme, A. H., and Miller, D. C. 1971, *Planet. Space Sci.*, **19**, 1229.
Eddington, A. 1910, *M.N.R.A.S.*, **70**, 442.
Finson, M. L., and Probstein, R. F. 1968, *Ap. J.*, **154**, 353.
Hanner, M. 1981, *Icarus*, **47**, 342.
Jambor, B. J. 1973, *Ap. J.*, **185**, 727.
Jewitt, D. C., and Meech, K. J. 1985, *Icarus*, **64**, 329.
Jewitt, D. C., Soifer, B. T., Neugebauer, G., Matthews, K., and Danielson, G. E. 1982, *A.J.*, **87**, 1854.
Meech, K. J., and Jewitt, D. C. 1987, in preparation.
Mukai, T. 1986, *Astr. Ap.*, **164**, 397.
Newburn, R. L., Jr., Bell, J. F., and McCord, T. B. 1981, *A.J.*, **86**, 469.
Oke, J. B., and Gunn, J. E. 1983, *Ap. J.*, **266**, 713.
Saito, K., Isobe, S., Nishioka, K., and Ishi, T. 1981, *Icarus*, **47**, 351.
Sekanina, Z., and Miller, F. D. 1973, *Science*, **179**, 565.
Wallace, L. V., and Miller, F. D. 1958, *A.J.*, **63**, 213.
Weaver, H. A., Feldman, P. D., Festou, M. C., A'Hearn, M. F., and Keller, H. U. 1981, *Icarus*, **47**, 449.

DAVID JEWITT and KAREN MEECH: 54-418, Department of Earth, Atmospheric, and Planetary Sciences, Massachusetts Institute of Technology, Cambridge, MA 02139

PLATE 15

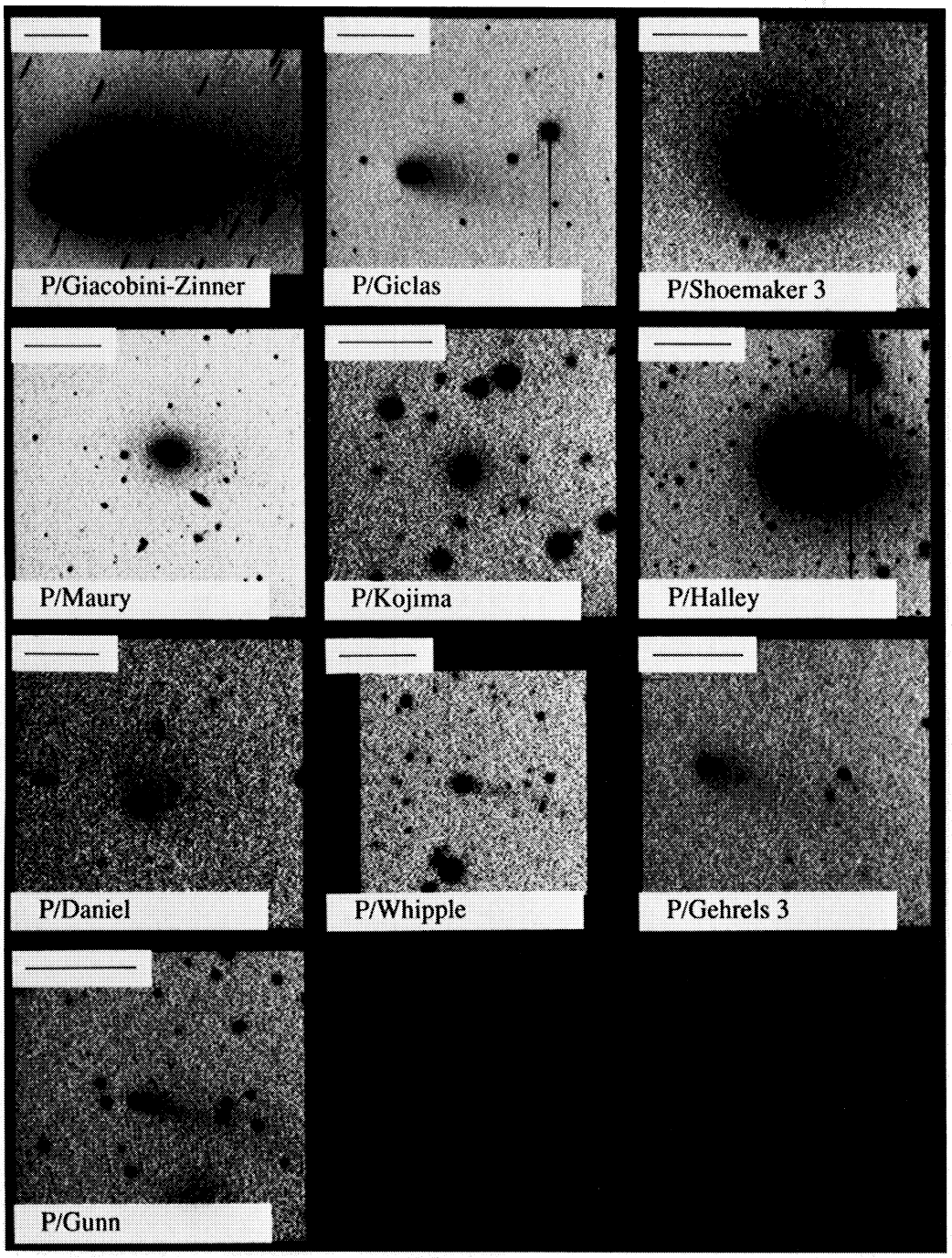

FIG. 1.—Charge-coupled device images of the 10 comets in this study. The comets are shown in order of increasing heliocentric distance. Each image is oriented with north at the top and east to the left. The scale bars indicate 30″.

JEWITT AND MEECH (*see* **317**, 993)